

NON-ERGODICITY OF THE NOSÉ-HOOVER THERMOSTATED HARMONIC OSCILLATOR

FRÉDÉRIC LEGOLL, MITCHELL LUSKIN, AND RICHARD MOECKEL

ABSTRACT. The Nosé-Hoover thermostat is a deterministic dynamical system designed for computing phase space integrals for the canonical Gibbs distribution. Newton's equations are modified by coupling an additional reservoir variable to the physical variables. The correct sampling of the phase space according to the Gibbs measure is dependent on the Nosé-Hoover dynamics being ergodic. Hoover presented numerical experiments that show the Nosé-Hoover dynamics to be non-ergodic when applied to the harmonic oscillator. In this article, we prove that the Nosé-Hoover thermostat does not give an ergodic dynamics for the one-dimensional harmonic oscillator when the "mass" of the reservoir is large. Our proof of non-ergodicity uses KAM theory to demonstrate the existence of invariant tori for the Nosé-Hoover dynamical system that separate phase space into invariant regions.

We present numerical experiments motivated by our analysis that seem to show that the dynamics is not ergodic even for a moderate thermostat mass. We also give numerical experiments of the Nosé-Hoover chain with two thermostats applied to the one-dimensional harmonic oscillator. These experiments seem to support the non-ergodicity of the dynamics if the masses of the reservoirs are large enough and are consistent with ergodicity for more moderate masses.

1. INTRODUCTION

Equilibrium statistical properties of molecular systems [3, 10] are given by phase space integrals of the form

$$\langle A \rangle = \int A(q, p) d\mu(q, p), \quad (1.1)$$

where $q = (q_1, \dots, q_M) \in \mathbb{R}^{nM}$ and $p = (p_1, \dots, p_M) \in \mathbb{R}^{nM}$ denote a set of positions $q_i \in \mathbb{R}^n$ and momenta $p_i \in \mathbb{R}^n$ of M particles (n denotes the space dimension), and $A(q, p)$ is an observable, a function defined over the phase space and related to the macroscopic quantity under study. If the molecular system is observed at fixed temperature θ , then the measure $d\mu$ is the Gibbs measure for the canonical ensemble [3, 10]

$$d\mu(q, p) = \left[\frac{\exp(-\beta H(q, p))}{\int \exp(-\beta H(q, p)) dq dp} \right] dq dp, \quad (1.2)$$

Date: March 24, 2006.

2000 Mathematics Subject Classification. 37M25, 65P10, 70F10, 82B80.

Key words and phrases. Nosé-Hoover, Nosé, invariant tori, molecular dynamics, sampling.

This work was supported in part by DMS-0304326, DMS-0500443, the Institute for Mathematics and Its Applications, and by the Minnesota Supercomputer Institute. This work is also based on work supported by the Department of Energy under Award Number DE-FG02-05ER25706.

where $H(q, p)$ is the Hamiltonian of the system and is often simply of the form

$$H(q, p) = \sum_{i=1}^M \frac{p_i^2}{2m_i} + V(q),$$

where $p_i^2 = p_i \cdot p_i$ and $V(q)$ is the potential energy. The parameter β that appears in (1.2) is related to the temperature θ by $\beta = 1/(k_B\theta)$, where k_B is the Boltzmann constant. In applications of interest, the number of particles is often very large ($M \geq 100,000$), hence computing integrals such as (1.1) is a challenging problem.

Molecular dynamics can be used to compute integrals such as (1.1). The method amounts to finding a dynamics on (q, p) which is ergodic with respect to the measure $d\mu$. As a consequence, the phase-space average (1.1) can be replaced by a time average

$$\int A(q, p) d\mu(q, p) = \frac{\int A(q, p) \exp(-\beta H(q, p)) dq dp}{\int \exp(-\beta H(q, p)) dq dp} = \lim_{T \rightarrow +\infty} \frac{1}{T} \int_0^T A(q(t), p(t)) dt \quad (1.3)$$

over a trajectory $(q(t), p(t))_{t \geq 0}$. The time average can be approximated by a formula such as

$$\lim_{T \rightarrow +\infty} \frac{1}{T} \int_0^T A(q(t), p(t)) dt \approx \lim_{N \rightarrow \infty} \frac{1}{N} \sum_{\ell=1}^N A(q_\ell, p_\ell),$$

where $(q_\ell, p_\ell)_{\ell \geq 1}$ is a numerical solution of the chosen dynamics.

To compute phase space integrals in the canonical ensemble, several deterministic dynamics have been proposed, such as the Nosé [12], the Nosé-Hoover [4], and the Nosé-Hoover chain dynamics [8]. More recently, the Nosé-Poincaré dynamics [1] and the Reversible Multiple Thermostat method [7] have been proposed. Stochastic dynamics (such as the Langevin equation) can also be considered, although we will not discuss them in the following.

The ergodicity condition has not been rigorously proven for any of the deterministic methods mentioned above. In fact, there is numerical evidence that shows that the Nosé and the Nosé-Hoover methods are not ergodic for some systems [4, 8, 14], including the one-dimensional harmonic oscillator. This article further explores non-ergodic behavior of the Nosé-Hoover dynamics in this simple example.

In Section 2, we present the Nosé-Hoover equations and we recall some of their properties. In Section 3, we prove that the Nosé-Hoover thermostat does not give an ergodic dynamics for the Gibbs measure (1.2) for the one-dimensional harmonic oscillator when the “mass” of the reservoir is large. Our method is to apply KAM theory, and more specifically Moser’s invariant curve theorem [13], to the Poincaré return map and to thus demonstrate the existence of invariant tori that separate phase space into invariant regions. Finally, in the last section, we present some numerical experiments with a Nosé-Hoover chain of two thermostats. For large reservoir masses, results show that the dynamics seems to be non ergodic. For moderate reservoir masses, they are consistent with ergodicity.

2. THE NOSÉ-HOOVER THERMOSTAT

The Nosé-Hoover dynamical system [4] is given by

$$\begin{aligned}\frac{dq_i}{dt} &= \frac{p_i}{m_i}, \\ \frac{dp_i}{dt} &= -\nabla_{q_i} V(q) - \frac{\xi}{Q} p_i, \\ \frac{d\xi}{dt} &= \sum_{i=1}^M \frac{p_i^2}{m_i} - nM\beta^{-1},\end{aligned}\tag{2.1}$$

where the phase space is described by the physical positions $q = (q_1, \dots, q_M) \in \mathbb{R}^{nM}$ and momenta $p = (p_1, \dots, p_M) \in \mathbb{R}^{nM}$ and an additional variable, ξ , which can be considered as the momentum of the thermostat. The constant Q , which is a parameter of the method, represents the mass of the reservoir and describes the strength of the coupling of the reservoir to the physical system. Let us note that, usually, a second additional variable is introduced [4]. This variable can be considered as the position of the thermostat. Since it is decoupled from all the other variables, we ignore it in the following.

We recall that for the canonical Gibbs measure $d\mu$ given by (1.2) we have

$$\int \sum_{i=1}^M \frac{p_i^2}{m_i} d\mu(q, p) = nM\beta^{-1},$$

so we have that

$$\lim_{T \rightarrow +\infty} \frac{1}{T} \int_0^T \sum_{i=1}^M \frac{p_i^2(t)}{m_i} dt = nM\beta^{-1}$$

for almost all initial conditions for any dynamics on (q, p) which is ergodic with respect to the measure $d\mu$. Thus, the right hand side of the Nosé-Hoover dynamical equation for $\frac{d\xi}{dt}$ is equal to twice the difference between the instantaneous kinetic energy of the physical system and the time-averaged kinetic energy of the physical system at temperature $\theta = k_B^{-1}\beta^{-1}$ with nM degrees of freedom. Hence, we see that if the kinetic energy of the physical system is too high for a sufficiently long time, then the “thermostat” added to the physical momentum equations applies a frictional force to damp the system. If the kinetic energy of the physical system is too low for a sufficiently long time, then the “thermostat” added to the physical momentum equations applies an “anti-frictional” force to add kinetic energy to the system.

The Nosé-Hoover system is not a Hamiltonian system and the Lebesgue measure $dq dp d\xi$ is not an invariant measure for the dynamics. Instead, the equations preserve a different measure which we will now describe. We recall that invariant measures $\rho(z)dz$ for a general dynamical system

$$\frac{dz}{dt} = f(z)$$

are determined by the equilibrium equation

$$\operatorname{div}(\rho(z)f(z)) = 0.\tag{2.2}$$

For the Nosé-Hoover system (2.1) with $z = (q, p, \xi)$, it is easy to check that

$$\rho(q, p, \xi) = \exp\left(-\beta \left[H(q, p) + \frac{\xi^2}{2Q} \right]\right)$$

satisfies the condition (2.2), so a normalized invariant measure for the Nosé-Hoover system (2.1) is given by

$$d\mu_{\text{NH}}(q, p, \xi) = \left[\frac{\exp\left(-\beta \left[H(q, p) + \frac{\xi^2}{2Q} \right]\right)}{\int \exp\left(-\beta \left[H(q, p) + \frac{\xi^2}{2Q} \right]\right) dq dp d\xi} \right] dq dp d\xi. \quad (2.3)$$

We recall that the flow of equations (2.1) is ergodic (or metrically indecomposable) with respect to the measure $d\mu_{\text{NH}}$ if the phase space, \mathbb{R}^3 , cannot be decomposed into two complementary invariant subsets, each with positive measure [5]. If the flow of (2.1) is ergodic with respect to the measure $d\mu_{\text{NH}}$, then given any integrable function $A \in L^1(d\mu_{\text{NH}})$ the Birkhoff ergodic theorem shows that for almost all initial conditions

$$\lim_{T \rightarrow +\infty} \frac{1}{T} \int_0^T A(q(t), p(t), \xi(t)) dt = \int A(q, p, \xi) d\mu_{\text{NH}}, \quad (2.4)$$

where $(q(t), p(t), \xi(t))$ is a solution of the Nosé-Hoover equations (2.1).

If $A = A(q, p)$ is an observable which depends only on the physical variables (q, p) , then

$$\int A(q, p) d\mu_{\text{NH}} = \int A(q, p) d\mu, \quad (2.5)$$

where $d\mu$ is the Gibbs measure (1.2). To see this, we observe from Fubini's Theorem that

$$\begin{aligned} \int A(q, p) d\mu_{\text{NH}} &= \frac{\int A(q, p) \exp\left(-\beta \left[H(q, p) + \frac{\xi^2}{2Q} \right]\right) dq dp d\xi}{\int \exp\left(-\beta \left[H(q, p) + \frac{\xi^2}{2Q} \right]\right) dq dp d\xi} \\ &= \frac{\int A(q, p) \exp(-\beta H(q, p)) dq dp \cdot \int \exp\left(-\beta \left[\frac{\xi^2}{2Q} \right]\right) d\xi}{\int \exp(-\beta H(q, p)) dq dp \cdot \int \exp\left(-\beta \left[\frac{\xi^2}{2Q} \right]\right) d\xi} \\ &= \int A(q, p) d\mu. \end{aligned} \quad (2.6)$$

We thus have that if the flow of (2.1) is ergodic with respect to the measure $d\mu_{\text{NH}}$ and if the observable $A = A(q, p)$ does not depend on ξ , then for almost all initial conditions we have from (2.4) that

$$\lim_{T \rightarrow +\infty} \frac{1}{T} \int_0^T A(q(t), p(t)) dt = \int A(q, p) d\mu = \frac{\int A(q, p) \exp(-\beta H(q, p)) dq dp}{\int \exp(-\beta H(q, p)) dq dp}, \quad (2.7)$$

where $(q(t), p(t), \xi(t))$ is a solution of the Nosé-Hoover equations (2.1).

This derivation has been made under the assumption that the Nosé-Hoover dynamics is ergodic with respect to the measure $d\mu_{\text{NH}}$. Numerical experiments show that the equality (2.7) does not always hold, even for long times T (in the limit of computationally reachable times). In particular, it is observed in [4, 8, 14] that if the system under consideration is a one-dimensional harmonic oscillator, that is, if $n = M = 1$, $m_1 = 1$, and $V(q) = \frac{1}{2}q^2$, then for lots of initial conditions, there exist c and C with $0 < c < C$ such that the corresponding solution of (2.1) satisfies

$$c \leq q^2(t) + p^2(t) \leq C \quad \text{for all } t. \quad (2.8)$$

This fact is observed for a wide range of values of Q , including $Q = 1$. This behavior contradicts (2.7), which gives in this case

$$\lim_{T \rightarrow +\infty} \frac{1}{T} \int_0^T A(q(t), p(t)) dt = \frac{\int A(q, p) \exp\left(-\beta \left(\frac{q^2 + p^2}{2}\right)\right) dq dp}{\int \exp\left(-\beta \left(\frac{q^2 + p^2}{2}\right)\right) dq dp}. \quad (2.9)$$

For example, if $A(q, p)$ is a positive function whose support lies in the disk $q^2 + p^2 < c$, the left-hand side of (2.9) will be zero while the right-hand side will be positive.

These numerical experiments give an indication that the Nosé-Hoover thermostated harmonic oscillator is not ergodic. In the next section we will give a rigorous proof of non-ergodicity if the reservoir mass Q is sufficiently large. We will apply KAM theory [13] to demonstrate the existence of invariant tori that separate the phase space into invariant regions of positive measure. The projections of these invariant regions to the (q, p) -plane satisfy inequalities of the form (2.8) and this explains the numerical observations. Motivated by our analysis, we show that we can find initial conditions such that the trajectory does not even sample the whole ring $\{(q, p) \in \mathbb{R}^2 : c \leq q^2 + p^2 \leq C\}$ for some $0 < c \leq C$, but only a part of it (see Figure 3 below).

3. INVARIANT TORI FOR THE NOSÉ-HOOVER HARMONIC OSCILLATOR DYNAMICS

We now write the Nosé-Hoover equations in the case of a one-dimensional harmonic oscillator. To simplify the notation, let us assume that the particle mass is $m_1 = 1$ and the target temperature is such that $\beta = 1/(k_B\theta) = 1$. In view of (2.1), the system of differential equations is given by

$$\begin{aligned} \dot{q} &= p, \\ \dot{p} &= -q - \epsilon^2 \xi p, \\ \dot{\xi} &= p^2 - 1, \end{aligned} \quad (3.1)$$

where $\epsilon = 1/\sqrt{Q}$.

We can introduce action-angle variables for the oscillator

$$q = \sqrt{2\tau} \cos \theta \quad \text{and} \quad p = -\sqrt{2\tau} \sin \theta \quad (3.2)$$

and rescale via $\alpha = \epsilon\xi$ to get:

$$\begin{aligned} \dot{\theta} &= 1 - \epsilon\alpha \sin \theta \cos \theta, \\ \dot{\tau} &= -2\epsilon\tau\alpha \sin^2 \theta, \\ \dot{\alpha} &= \epsilon(2\tau \sin^2 \theta - 1). \end{aligned} \quad (3.3)$$

These equations preserve the volume element

$$d\Omega = \lambda(\tau, \alpha) d\theta d\tau d\alpha,$$

where

$$\lambda(\tau, \alpha) = e^{-\tau - \alpha^2/2}.$$

We now make a change of variables as in the averaging method [13]. Setting

$$\tau = \hat{\tau} + \epsilon \hat{\tau} \hat{\alpha} \sin \theta \cos \theta \quad \text{and} \quad \alpha = \hat{\alpha} - \epsilon \hat{\tau} \sin \theta \cos \theta$$

gives a new ODE of the form:

$$\begin{aligned}\dot{\theta} &= 1 - \epsilon \hat{\alpha} \sin \theta \cos \theta + O(\epsilon^2), \\ \dot{\hat{\tau}} &= -\epsilon \hat{\tau} \hat{\alpha} + O(\epsilon^2), \\ \dot{\hat{\alpha}} &= \epsilon(\hat{\tau} - 1) + O(\epsilon^2).\end{aligned}\tag{3.4}$$

The displayed terms in $\dot{\hat{\tau}}, \dot{\hat{\alpha}}$ are the averages with respect to θ of the corresponding terms in (3.3). These equations preserve the volume element obtained by transforming $d\Omega$:

$$d\hat{\Omega}_\epsilon = \hat{\lambda}_\epsilon(\theta, \hat{\tau}, \hat{\alpha}) d\theta d\hat{\tau} d\hat{\alpha},$$

where

$$\hat{\lambda}_\epsilon(\theta, \hat{\tau}, \hat{\alpha}) = e^{-\hat{\tau} - \hat{\alpha}^2/2} + O(\epsilon).$$

Indeed,

$$\begin{aligned}\hat{\lambda}_\epsilon(\theta, \hat{\tau}, \hat{\alpha}) &= e^{-\tau - \alpha^2/2} \left| \frac{\partial(\tau, \alpha)}{\partial(\hat{\tau}, \hat{\alpha})} \right| \\ &= e^{-\tau - \alpha^2/2} \left(1 + \frac{\epsilon}{2} \hat{\alpha} \sin 2\theta + \frac{\epsilon^2}{4} \hat{\tau} \sin^2 2\theta \right) \\ &= e^{-\hat{\tau} - \hat{\alpha}^2/2} e^{-\frac{1}{2}\epsilon^2 \hat{\tau}^2 \sin^2 \theta \cos^2 \theta} \left(1 + \frac{\epsilon}{2} \hat{\alpha} \sin 2\theta + \frac{\epsilon^2}{4} \hat{\tau} \sin^2 2\theta \right) \\ &= e^{-\hat{\tau} - \hat{\alpha}^2/2} + O(\epsilon).\end{aligned}$$

In what follows, the $\hat{\cdot}$ will be suppressed and the new variables will again be called (θ, τ, α) .

We will apply the KAM theory [13] to the Poincaré return map P_ϵ of the plane $\Sigma = \{(\theta, \tau, \alpha) : \theta = 0 \bmod 2\pi\}$ for the ODE (3.4). This map preserves the area-element:

$$d\omega_\epsilon = \lambda_\epsilon^0(\tau, \alpha) d\tau d\alpha,\tag{3.5}$$

with $\lambda_\epsilon^0(\tau, \alpha) = \lambda_\epsilon(0, \tau, \alpha) = e^{-\tau - \alpha^2/2}$.

This can be shown as follows. Consider a small rectangle $D \subset \Sigma$ with dimensions $\delta\tau\delta\alpha$ centered at some point $(0, \tau_0, \alpha_0) \in \Sigma$. Form a three-dimensional tube \mathcal{T} by following the solutions of the ODE (3.4) until they reach the plane $\theta = 2\pi$. One end of the tube will be the rectangle D and the other will be its image $P_\epsilon(D)$ under the Poincaré map.

Following \mathcal{T} forward under the flow of the ODE for a time δt produces a new tube \mathcal{T}' and the volumes of \mathcal{T} and \mathcal{T}' with respect to the volume element $d\Omega_\epsilon$ are equal. Now \mathcal{T} and \mathcal{T}' differ by two small solid ‘‘cylinders’’ with bases D and $P_\epsilon(D)$, respectively. Let $\delta = \max(|\delta\tau|, |\delta\alpha|, |\delta t|)$. Then the volume of the cylinder over D is

$$\lambda_\epsilon(0, \tau_0, \alpha_0) \delta\tau \delta\alpha \delta\theta + O(\delta^4) = \lambda_\epsilon(0, \tau_0, \alpha_0) \dot{\theta}(0, \tau_0, \alpha_0) \delta\tau \delta\alpha \delta t + O(\delta^4),$$

where $\dot{\theta}$ is the first component of the vectorfield (3.4). On the other hand, the volume of the cylinder over $P_\epsilon(D)$ is

$$\lambda_\epsilon(2\pi, \tau_1, \alpha_1) |DP_\epsilon(\tau_0, \alpha_0)| \delta\tau \delta\alpha \delta\theta + O(\delta^4) = \lambda_\epsilon(2\pi, \tau_1, \alpha_1) \dot{\theta}(2\pi, \tau_1, \alpha_1) |DP_\epsilon(\tau_0, \alpha_0)| \delta\tau \delta\alpha \delta t + O(\delta^4)$$

where $P_\epsilon(\tau_0, \alpha_0) = (\tau_1, \alpha_1)$ and where $|DP_\epsilon(\tau_0, \alpha_0)|$ is the Jacobian determinant of the Poincaré map. Note that $\dot{\theta}(0, \tau, \alpha) = \dot{\theta}(2\pi, \tau, \alpha) = 1$ since this holds for the ODE (3.3) and is preserved by the coordinate change leading to (3.4). It then follows from letting $\delta \rightarrow 0$ that

$$\lambda_\epsilon(0, \tau_0, \alpha_0) = |DP_\epsilon(\tau_0, \alpha_0)| \lambda_\epsilon(2\pi, \tau_1, \alpha_1)$$

which proves that the Poincaré map P_ϵ preserves the area element $\lambda_\epsilon^0(\tau, \alpha) d\tau d\alpha$ as claimed.

We will use the version of Moser's invariant curve theorem from "Lectures on Celestial Mechanics" by Siegel and Moser [13, sections 32–34]. That theorem starts with a real-analytic map P of the form

$$\begin{aligned}x_1 &= x + \gamma y + f(x, y), \\y_1 &= y + g(x, y),\end{aligned}\tag{3.6}$$

where f and g are periodic in x with period 2π . In the application they have in mind, x and y are respectively the angle and radius in a polar coordinate system near a fixed point. If $f = g = 0$, then the map reduces to a standard twist map where the radial variable is preserved while the angular variable is rotated by an amount which depends on the radius. They assume a *twist condition*, $\gamma \neq 0$, so the amount of rotation really does change. The theorem shows that if f and g are small, then some of these invariant circles will persist.

In order to prove this, they also assume that P satisfies the *curve-intersection property*. This means that for any simple closed curve, C , of the form

$$y = \psi(x) \quad \text{where} \quad \psi(x + 2\pi) = \psi(x),$$

we have that $C \cap P(C) \neq \emptyset$.

Such a curve represents a simple closed curve around the fixed point for the map before changing to polar coordinates. If this map preserves an area element, then such a loop cannot map completely inside or completely outside itself and so the curve intersection property will hold.

To state the theorem precisely, fix an annulus $a \leq y \leq b$ with $b - a = 1$ (this condition can always be achieved by rescaling y). Since f and g are real analytic, they extend to complex analytic functions on some complex neighborhood D of $\mathbb{R} \times [a, b]$ in \mathbb{C}^2 . We also specify a so-called *Diophantine condition* on the rotation numbers of the unperturbed circles. Recall that if $f(x)$ satisfies $f(x + 2\pi) = f(x) + 2\pi$ and defines a homeomorphism of the circle $\mathbb{R} \bmod 2\pi$, then the rotation number $\omega = \lim_{n \rightarrow \infty} \frac{1}{2\pi n} (f^n(x) - x)$ exists and is independent of the initial condition, x . For the unperturbed circles of constant y we have $f^n(x) - x = n\gamma y$, so $\omega = \frac{\gamma y}{2\pi}$. Fix any constants $c_0 > 0$ and $\mu \geq 2$ and consider rotation numbers satisfying:

$$|l\omega - k| = \left| \frac{l\gamma y}{2\pi} - k \right| \geq \frac{\gamma c_0}{l^\mu} \quad \text{for all } k, l \in \mathbb{Z}, l > 0.\tag{3.7}$$

It is shown in Siegel-Moser that for c_0 sufficiently small, the set of y which satisfy this condition forms a positive measure Cantor set in the interval $[a, b]$ whose measure tends to $b - a = 1$ as $c_0 \rightarrow 0$. Moser's theorem states that if f and g are sufficiently small, then for each such y there is a nearby invariant curve of P with the same rotation number. More precisely,

Theorem 3.1. *Let P be a real analytic map of the form (3.6) which extends to a complex domain D . Assume that P is periodic in x of period 2π and has the curve intersection property. Fix a Diophantine condition (3.7) and an annulus $a \leq y \leq b$ where $b - a = 1$.*

Given any $\tilde{\epsilon} > 0$ there is a $\delta > 0$ such that if

$$|f| + |g| < \delta\gamma,\tag{3.8}$$

then for every $y_0 \in [a, b]$ which satisfies (3.7), P has an invariant curve of the form $y = \psi(x)$ where $\psi(x + 2\pi) = \psi(x)$ with $|\psi(x) - y_0| < \tilde{\epsilon}$ for all x . Moreover, the restriction of P to this curve has rotation number $\omega = \frac{\gamma y_0}{2\pi}$. Here $|\cdot|$ denotes the sup norm in the complex domain D . The constant δ depends on $c_0, \mu, \tilde{\epsilon}, D$ but not on γ .

To apply this result to P_ϵ , some further coordinate changes will be needed. First, note that

$$P_\epsilon(\tau, \alpha) = Q_\epsilon(\tau, \alpha) + O(\epsilon^2),$$

where Q_ϵ is the time- 2π advance map of the differential equation:

$$\begin{aligned}\dot{\tau} &= -\epsilon\tau\alpha, \\ \dot{\alpha} &= \epsilon(\tau - 1),\end{aligned}$$

or equivalently, the time- $2\pi\epsilon$ advance map of

$$\begin{aligned}\tau' &= -\tau\alpha, \\ \alpha' &= \tau - 1.\end{aligned}\tag{3.9}$$

This follows because the return time to the section Σ is

$$T(\tau, \alpha) = 2\pi + O(\epsilon).$$

The ODE (3.9) has an integral

$$G(\tau, \alpha) = \tau - \ln \tau + \frac{1}{2}\alpha^2 - 1.\tag{3.10}$$

Furthermore there is an equilibrium point at $(\tau_0, \alpha_0) = (1, 0)$ on the level set $G = 0$. All of the other level sets in the half-plane $\tau > 0$ are simple closed curves around the equilibrium point (see Figure 1). These are all invariant curves for the map Q_ϵ , and the goal is to show that the actual Poincaré maps P_ϵ with ϵ sufficiently small also have such invariant curves. We note that the existence of invariant curves for P_ϵ corresponds to the existence of invariant tori for the 3D flow of (3.4). These tori separate the phase space into invariant 3D regions, showing that the flow is not ergodic. Note that for an invariant torus close to a level set $G = g_0 > 0$ we have

$$\tau - \ln \tau \leq 1 + g_0 + O(\epsilon).$$

Since $\tau = \frac{1}{2}(p^2 + q^2)$, it follows easily that the projection of the torus to the (q, p) -plane satisfies bounds of the form (2.8).

It is worth noting that even without using the KAM theory, the existence of the integral G for the averaged system (3.9) shows that the convergence of ergodic averages in (2.9) would be slow for ϵ small. Indeed, the standard averaging theory shows that the trajectories of the actual system remain ϵ close to those of the averaged system on a time scale of order $1/\epsilon$. The KAM theory shows that the trajectories which lie on the invariant tori are close to the averaged ones for *all* time. Moreover, other trajectories are trapped between the tori and so their G coordinates are prevented from wandering very far.

To get the Poincaré map into the form (3.6), we introduce action-angle variables around the equilibrium point. The integral G provides a natural radial coordinate or action variable. To construct the corresponding angle variable, let $T(g)$ denote the period of the periodic solutions of (3.9) which correspond to the level curve $G = g$. We define an angular coordinate ϕ to be the time along this orbit multiplied by $2\pi/T(g)$, taking the initial point $\phi = 0$ along the τ -axis to the right of the equilibrium point. By definition, the ODE (3.9) will become:

$$\begin{aligned}\phi' &= 2\pi/T(G), \\ G' &= 0,\end{aligned}$$

in these coordinates and so the time- $2\pi\epsilon$ advance map $Q_\epsilon(\phi, G) = (\phi_1, G_1)$ is

$$\begin{aligned}\phi_1 &= \phi + 2\pi\epsilon/T(G), \\ G_1 &= G.\end{aligned}\tag{3.11}$$

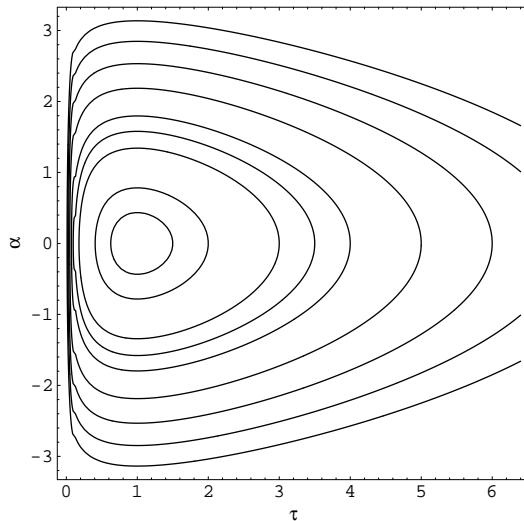


FIGURE 1. Level curves of G (see (3.10)), the integral for the averaged equations (3.9).

The Poincaré maps P_ϵ can be viewed as $O(\epsilon^2)$ perturbations of (3.11). To see this, let us first show that P_ϵ has a fixed point $(\tau_\epsilon, \alpha_\epsilon) = (1, 0) + O(\epsilon)$. Since Q_ϵ is the time- $2\pi\epsilon$ advance map of (3.9), we compute that

$$Q_\epsilon(\tau, \alpha) = (\tau - 2\pi\epsilon\tau\alpha, \alpha + 2\pi\epsilon(\tau - 1)) + O(\epsilon^2),$$

hence

$$P_\epsilon(\tau, \alpha) - (\tau, \alpha) = 2\pi\epsilon R(\epsilon, \tau, \alpha), \quad (3.12)$$

with

$$R(\epsilon, \tau, \alpha) = (-\tau\alpha + \epsilon u(\epsilon, \tau, \alpha), \tau - 1 + \epsilon v(\epsilon, \tau, \alpha))$$

for some smooth functions u and v . We then apply the implicit function theorem to $R(\epsilon, \tau, \alpha)$ to continue the solution in ϵ from $R(0, 1, 0) = 0$. We can compute

$$\frac{\partial R}{\partial(\tau, \alpha)}(0, \tau, \alpha) = \begin{pmatrix} -\alpha & -\tau \\ 1 & 0 \end{pmatrix},$$

so the matrix $\frac{\partial R}{\partial(\tau, \alpha)}(0, 1, 0)$ is invertible. As a consequence, the implicit equation $R(\epsilon, \tau_\epsilon, \alpha_\epsilon) = 0$ defines a function $\epsilon \mapsto (\tau_\epsilon, \alpha_\epsilon)$ from a neighborhood of 0 to a neighborhood of $(1, 0)$. In view of (3.12), we see that $(\tau_\epsilon, \alpha_\epsilon)$ is a fixed point of P_ϵ . From the equation $R(\epsilon, \tau_\epsilon, \alpha_\epsilon) = 0$, we obtain that $(\tau_\epsilon, \alpha_\epsilon) = (1, 0) + O(\epsilon)$.

After a translation of the coordinates, one can assume that all maps P_ϵ for ϵ sufficiently small fix the point $(1, 0)$. Now use the same coordinates (ϕ, G) as for the unperturbed map Q_ϵ . G is not an integral but one has that $P_\epsilon(\phi, G) = (\phi_1, G_1)$ with

$$\begin{aligned} \phi_1 &= \phi + 2\pi\epsilon/T(G) + O(\epsilon^2), \\ G_1 &= G + O(\epsilon^2). \end{aligned} \quad (3.13)$$

The fact that P_ϵ preserves the area element $d\omega_\epsilon$ (see (3.5)) implies that (3.13) satisfies the curve-intersection property. We also need a twist condition on the period $T(G)$. It will be shown below that $T'(G) > 0$, that is, the period of the periodic solutions increases as we move out from the

equilibrium point. This implies that one can replace the action coordinate G by the period $T(G)$ or its reciprocal $1/T(G)$. To match the notation in Siegel-Moser, let $y = 1/T(G)$ and $x = \phi$. Then one finds that the Poincaré maps take the form

$$\begin{aligned} x_1 &= x + 2\pi\epsilon y + \epsilon^2 \tilde{f}(x, y, \epsilon), \\ y_1 &= y + \epsilon^2 \tilde{g}(x, y, \epsilon). \end{aligned} \tag{3.14}$$

This is of the form (3.6) with $\gamma = 2\pi\epsilon$ and with the perturbing functions $f = \epsilon^2 \tilde{f}$ and $g = \epsilon^2 \tilde{g}$ of order $O(\epsilon^2)$.

We are now in a position to apply Moser's theorem to obtain:

Theorem 3.2. *Fix an annulus \mathcal{A} of the form $c \leq G \leq d$ with $0 < c < d$. Then for ϵ sufficiently small, the Poincaré map P_ϵ of the Nosé-Hoover system has infinitely many invariant curves close to the level curves of G in \mathcal{A} . In particular, the corresponding flow is not ergodic.*

The proof consists in checking the remaining hypotheses of Moser's theorem. Note that the differential equation (3.4) is real-analytic in $(\theta, \tau, \alpha, \epsilon)$. It follows that the Poincaré map $P_\epsilon(\tau, \alpha)$ is real-analytic in (τ, α, ϵ) . The location of the fixed point $(\tau_\epsilon, \alpha_\epsilon)$ is a real-analytic function of ϵ (for ϵ sufficiently small) and so composing the Poincaré map with a translation to move this point to $(1, 0)$ preserves analyticity. The action angle variables (ϕ, G) are independent of ϵ and are real-analytic in (τ, α) away from the fixed point itself. Finally, the period function $T(G)$ is analytic in G . Thus the map (3.14) is real-analytic with respect to (x, y, ϵ) for $0 < y < Y$, $|\epsilon| < \epsilon_0$ where $Y > 0, \epsilon_0 > 0$ are constants. Since x is an angular variable, the map is also periodic with respect to x with period 2π .

The annulus \mathcal{A} contains an annulus of the form $0 < a \leq y \leq b < Y$. If $b - a = k \neq 1$, then we can set $y = y'/k$ where y' is a new variable. The map will retain the same form except that $\gamma = 2\pi\epsilon$ is replaced by $\gamma' = 2\pi\epsilon/k$. Once a and b are fixed, the Poincaré map admits a complex-analytic extension to some domain of the form $E = D \times \{|\epsilon| \leq \epsilon_1\} \subset \mathbb{C}^3$ where D is a closed δ -neighborhood of $\mathbb{R} \times [a, b]$ in \mathbb{C}^2 , and $\delta > 0, \epsilon_1 > 0$ are constants. For any fixed choice of ϵ with $|\epsilon| \leq \epsilon_1$, the perturbing functions \tilde{f} and \tilde{g} in (3.14) will have complex analytic extensions to D . We now fix the Diophantine constants c_0 and μ in (3.7) and choose any $\tilde{\epsilon} > 0$. Letting $\delta > 0$ be the constant in (3.8) guaranteed by Moser's theorem, the theorem shows that for any $y_0 \in [a, b]$ satisfying (3.7), and for any real analytic functions f, g with complex extensions to D which satisfy (3.8), the corresponding map admits an invariant curve $\tilde{\epsilon}$ -close to $y = y_0$.

We now let $f = \epsilon^2 \tilde{f}$ and $g = \epsilon^2 \tilde{g}$ where we think of ϵ as fixed, and we let $K = \sup_E |\tilde{f}| + |\tilde{g}|$. Then $|f| + |g| \leq \epsilon^2 K$ on D . Since $\gamma = 2\pi\epsilon$ (or $\gamma' = 2\pi\epsilon/k$), it follows that (3.8) holds for all ϵ sufficiently small.

To complete the proof, it only remains to verify that the period satisfies $T'(G) > 0$. We first introduce a new variable $\sigma = \ln \tau$. Then (3.9) becomes:

$$\begin{aligned} \sigma' &= -\alpha, \\ \alpha' &= e^\sigma - 1, \end{aligned} \tag{3.15}$$

which is a planar Hamiltonian system with Hamiltonian function

$$G(\sigma, \alpha) = \frac{1}{2}\alpha^2 + e^\sigma - 1 - \sigma.$$

In fact, it is of the classical kinetic plus potential form with potential

$$V(\sigma) = e^\sigma - 1 - \sigma$$

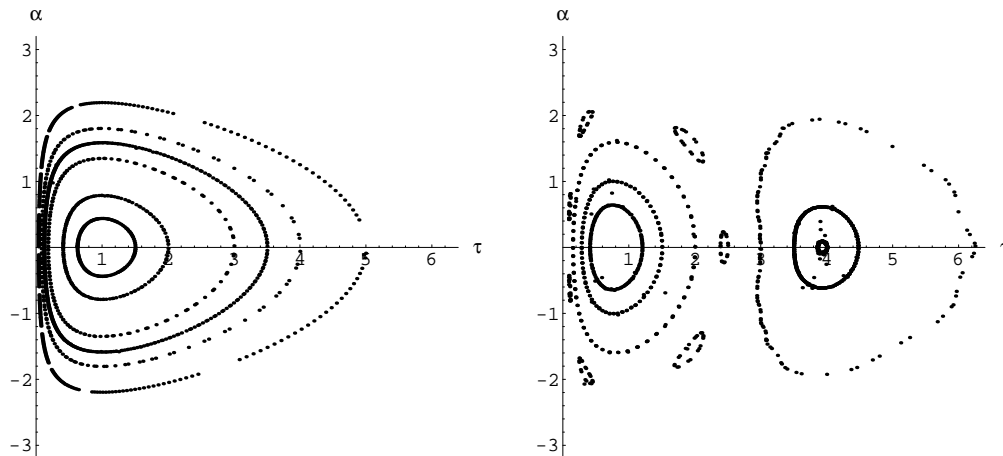


FIGURE 2. Numerically computed orbits of the Poincaré map of the plane $\theta = 0 \bmod 2\pi$ for the ODE (3.3); $\epsilon = 0.1$ (left) and $\epsilon = 1.0$ (right).

(except that in the ODE (3.15), σ plays the role of the momentum variable and α the role of the position). The equilibrium point is now at $(\sigma, \alpha) = (0, 0)$.

The behavior of the period as a function of energy for such systems is a well-studied problem. A result of Chicone [2] shows that $T(G)$ will be a strictly increasing function of energy G provided that $\frac{V(\sigma)}{(V'(\sigma))^2}$ is a strictly convex function (except at $\sigma = 0$). This condition reads

$$6VV''^2 - 3V'^2V''' - 2VV'V'' > 0,$$

except at $\sigma = 0$. It is not hard to check that this is true for the potential $V(\sigma)$ above.

Figure 2 shows numerically computed Poincaré maps of the ODE (3.3) for two values of ϵ . The Poincaré map for $\epsilon = 0.1$ has invariant curves close to the level curves of G in Figure 1. Apparently the Poincaré map for $\epsilon = 1$ still has many invariant curves although they are not particularly close to the level curves of G . If these really do exist, then the Nosé-Hoover system is non-ergodic even for $\epsilon = 1$.

It is interesting to remark that, for $\epsilon = 1$, the Poincaré map invariant curves are sometimes composed of a set of islands (instead of being simple closed curves). This is the case for instance with the initial condition $(\theta, \tau, \alpha) = (0, 2.42, 0)$ which corresponds to $(q, p, \xi) = (2.2, 0, 0)$ (7 islands can be seen on the right hand side of Figure 2). Starting from this initial condition, we numerically integrate (3.1) with a time step $\Delta t = 0.001$ for $5 \cdot 10^7$ time steps with the algorithm proposed in [9]. This second-order algorithm is based on an operator splitting technique. It preserves the measure (2.3) as well as the time-reversibility of (3.1). Figure 3 shows the projection of the time trajectory of the (q, p) -plane. With this initial condition, the trajectory seems not even to sample a ring of the form $\{(q, p) \in \mathbb{R}^2 : c \leq q^2 + p^2 \leq C\}$ for some $0 < c \leq C$, but only a part of it.

4. HARMONIC OSCILLATOR COUPLED WITH A NOSÉ-HOOVER CHAIN

In the previous section, we have proven that a one-dimensional harmonic oscillator coupled to a Nosé-Hoover thermostat is not an ergodic system with respect to the Gibbs measure, when the mass Q of the reservoir is large. As mentioned above, numerical observations of this fact have

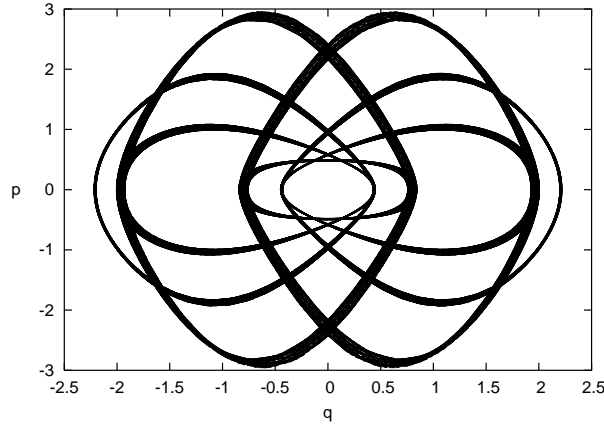


FIGURE 3. Projection on the (q, p) -plane of the numerically computed trajectory of (3.1) with $\epsilon = 1$, starting from the initial condition $(q, p, \xi) = (2.2, 0, 0)$.

already been reported in [4, 8, 14], even for moderate values of Q such as $Q = 1$. As a consequence, it is known that one should be cautious when making use of the Nosé-Hoover equations (2.1) to compute phase space integrals such as (1.1).

One way that has been proposed to circumvent this difficulty is to generalize the Nosé-Hoover equations to the so-called Nosé-Hoover chain equations [8]. The idea consists in coupling the physical variables (q, p) with a first thermostat as in (2.1) and to then couple this thermostat with a second one, which can be coupled to a third one, and so on. The variables now include M_{ext} additional scalar variables, ξ_j for $j = 1, \dots, M_{\text{ext}}$, where the number M_{ext} of thermostats can be freely specified. The Nosé-Hoover chain dynamics is given by

$$\begin{aligned}
 \frac{dq_i}{dt} &= \frac{p_i}{m_i}, \\
 \frac{dp_i}{dt} &= -\nabla_{q_i} V - \frac{\xi_1}{Q_1} p_i, \\
 \frac{d\xi_1}{dt} &= \left(\sum_{i=1}^M \frac{p_i^2}{m_i} - nM\beta^{-1} \right) - \frac{\xi_2}{Q_2} \xi_1, \\
 \frac{d\xi_j}{dt} &= \left(\frac{\xi_{j-1}^2}{Q_{j-1}} - \beta^{-1} \right) - \frac{\xi_{j+1}}{Q_{j+1}} \xi_j \quad \text{for } j = 2, \dots, M_{\text{ext}} - 1, \\
 \frac{d\xi_{M_{\text{ext}}}}{dt} &= \frac{\xi_{M_{\text{ext}}-1}^2}{Q_{M_{\text{ext}}-1}} - \beta^{-1},
 \end{aligned} \tag{4.1}$$

where the masses $Q_1, \dots, Q_{M_{\text{ext}}}$ are free parameters that can be arbitrarily specified.

For the Nosé-Hoover system (4.1) with $z = (q, p, \xi_1, \dots, \xi_{M_{\text{ext}}})$, it is easy to check that

$$\rho(q, p, \xi_1, \dots, \xi_{M_{\text{ext}}}) = \exp \left(-\beta \left[H(q, p) + \sum_{j=1}^{M_{\text{ext}}} \frac{\xi_j^2}{2Q_j} \right] \right)$$

satisfies the condition (2.2), so an invariant measure for the Nosé-Hoover system (4.1) is given by

$$d\mu_{\text{NHC}}(q, p, \xi_1, \dots, \xi_{M_{\text{ext}}}) = \frac{\exp\left(-\beta \left[H(q, p) + \sum_{j=1}^{M_{\text{ext}}} \frac{\xi_j^2}{2Q_j} \right]\right) dq dp d\xi_1 \dots d\xi_{M_{\text{ext}}}}{\int \exp\left(-\beta \left[H(q, p) + \sum_{j=1}^{M_{\text{ext}}} \frac{\xi_j^2}{2Q_j} \right]\right) dq dp d\xi_1 \dots d\xi_{M_{\text{ext}}}}. \quad (4.2)$$

We can now calculate that

$$\int \sum_{i=1}^M \frac{p_i^2}{m_i} d\mu_{\text{NHC}} = nM\beta^{-1},$$

and

$$\int \frac{\xi_j^2}{Q_j} d\mu_{\text{NHC}} = \beta^{-1} \quad \text{for } j = 1, \dots, M_{\text{ext}}.$$

Hence, we can see that the evolution of ξ_1 in (4.1) is controlled by the difference between the instantaneous value of twice the kinetic energy $\sum_{i=1}^M \frac{p_i^2}{m_i}$ and its average value with respect to the invariant measure $d\mu_{\text{NHC}}$ and the evolution of ξ_j for $j = 2, \dots, M_{\text{ext}}$ in (4.1) is controlled by the difference between the instantaneous value of twice the “kinetic energy” ξ_{j-1}^2/Q_{j-1} and its average value with respect to the invariant measure $d\mu_{\text{NHC}}$.

If (4.1) is ergodic with respect to $d\mu_{\text{NHC}}$, computations similar to the ones performed in Section 2 show that

$$\lim_{T \rightarrow +\infty} \frac{1}{T} \int_0^T A(q(t), p(t)) dt = \int A(q, p) d\mu(q, p), \quad (4.3)$$

where $(q(t), p(t), \xi_1(t), \dots, \xi_{M_{\text{ext}}}(t))$ is a solution of the Nosé-Hoover chain dynamics and $d\mu(q, p)$ is the Gibbs measure (1.2). Hence, the Nosé-Hoover chain dynamics can be used to compute phase space integrals in the canonical ensemble if (4.1) is ergodic with respect to $d\mu_{\text{NHC}}$.

In this section, we numerically study the case of a one-dimensional harmonic oscillator coupled to a Nosé-Hoover chain of length $M_{\text{ext}} = 2$. We consider the case $Q_1 = Q_2$. In view of (4.1), the dynamics reads

$$\begin{aligned} \dot{q} &= p, \\ \dot{p} &= -q - \epsilon^2 p \xi_1, \\ \dot{\xi}_1 &= p^2 - 1 - \epsilon^2 \xi_1 \xi_2, \\ \dot{\xi}_2 &= \epsilon^2 \xi_1^2 - 1, \end{aligned} \quad (4.4)$$

where $\epsilon = 1/\sqrt{Q_1} = 1/\sqrt{Q_2}$. We again introduce the action-angle variables (τ, θ) for the oscillator (see (3.2)) and rescale via $\alpha_j = \epsilon \xi_j$ to get

$$\begin{aligned} \dot{\theta} &= 1 - \epsilon \alpha_1 \sin \theta \cos \theta, \\ \dot{\tau} &= -2\epsilon \tau \alpha_1 \sin^2 \theta, \\ \dot{\alpha}_1 &= \epsilon(2\tau \sin^2 \theta - 1 - \alpha_1 \alpha_2), \\ \dot{\alpha}_2 &= \epsilon(\alpha_1^2 - 1). \end{aligned} \quad (4.5)$$

For small ϵ , the corresponding averaged system reads after rescaling time,

$$\begin{aligned}\dot{\tau} &= -\tau\alpha_1, \\ \dot{\alpha}_1 &= \tau - 1 - \alpha_1\alpha_2, \\ \dot{\alpha}_2 &= \alpha_1^2 - 1.\end{aligned}\tag{4.6}$$

In the case of the Nosé-Hoover equation, the averaged system is (3.9), and the analysis conducted in Section 3 is based on the knowledge of a first integral for (3.9), namely the function $G(\tau, \alpha)$ defined by (3.10). In the case of (4.6), we were not able to find such a first integral. Let us follow a different route and study the system by numerically computing the Poincaré return map of the plane $\Sigma_{\text{NHC}}^{\text{av}} = \{(\tau, \alpha_1, \alpha_2) : \alpha_2 = 0\}$ for the ODE (4.6). Two trajectories of the return map with different initial conditions are shown in Figure 4. Some initial conditions lead to trajectories which lie on invariant curves (see right-hand side of Figure 4) and the corresponding values of τ that are sampled are bounded from below and isolated from 0: there exists $\tau_c^{\epsilon=0} > 0$ such that for all t we have $\tau(t) \geq \tau_c^{\epsilon=0}$. For other initial conditions, the trajectory does not seem to be confined to a curve (see left-hand side of Figure 4), but it still does not sample the entire plane.

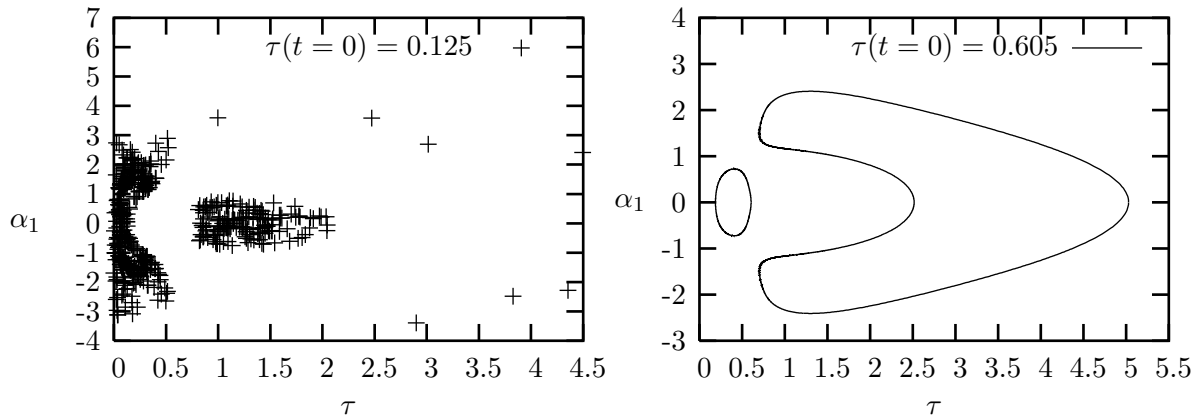


FIGURE 4. Numerically computed orbits of the Poincaré return map of the plane $\alpha_2 = 0$ for the ODE (4.6). Left: the initial condition is $(\tau, \alpha_1, \alpha_2) = (q_0^2/2, 0, 0)$ with $q_0 = 0.5$; a similar trajectory is obtained for $q_0 = 1.3$ and $q_0 = 1.5$. Right: the initial condition is $(\tau, \alpha_1, \alpha_2) = (q_0^2/2, 0, 0)$ with $q_0 = 1.1$; a similar trajectory is obtained for $q_0 = 0.65, 0.7, 0.75, 0.8, 0.85, 0.9, 0.95$ and 1.0 .

We now consider the ODE (4.5) and study whether the behaviour we observe in the case $\epsilon \rightarrow 0$ still persists in the case of a small but positive ϵ . We choose $Q_1 = Q_2 = 10$, that is $\epsilon = 1/\sqrt{10} = 0.316$, and we numerically integrate (4.4) with the second-order algorithm proposed in [9] from the initial condition $(q, p, \xi_1, \xi_2) = (1.1, 0, 0, 0)$. This condition corresponds to an initial condition for which the Poincaré return map of (4.6) seems to have invariant curves (see Figure 4, right-hand side). Figure 5 shows the trace of the time trajectory of (4.5) on the plane $\Sigma_{\text{NHC}} = \{(\theta, \tau, \alpha_1, \alpha_2) : \alpha_2 = 0\}$. We can see the topological similarity between curves on Figures 4 (right-hand side) and 5, although they are quantitatively quite different. Figure 6 shows the projection of the same trajectory on the (q, p) -plane. We see that the values of (q, p) that are sampled still satisfy $\tau(t) = (q^2(t) + p^2(t))/2 \geq \tau_c^\epsilon$ for some $\tau_c^\epsilon > 0$ and all $t \geq 0$. Thus, the lower bound on the values of τ that we observe for the averaged dynamics persists in the case $\epsilon = 1/\sqrt{10}$. For the initial condition we consider here, $\tau_c^{\epsilon=0} = 0.188$ whereas $\tau_c^\epsilon = 0.194$. Because of this lower bound, we obtain a contradiction with (4.3), and hence this numerical experiment indicates that a one-dimensional

harmonic oscillator coupled to a Nosé-Hoover chain of two thermostats is not always an ergodic system. We observe this non-ergodicity for many different initial conditions (including all those listed in Figure 4), and for many different values of $Q \geq 10$.

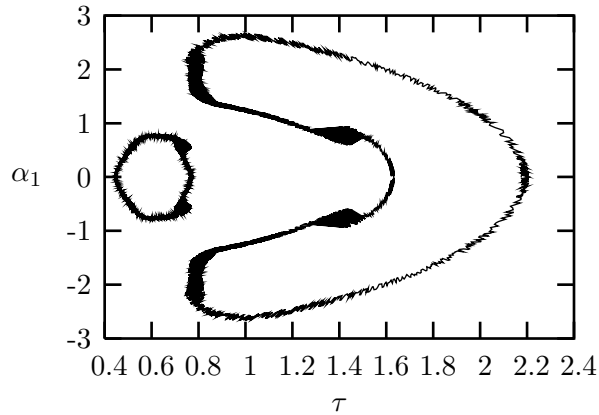


FIGURE 5. Trace of the trajectory of (4.5) with $\epsilon = 1/\sqrt{10}$ on the plane $\alpha_2 = 0$. The initial condition is $(\theta, \tau, \alpha_1, \alpha_2) = (0, q_0^2/2, 0, 0)$ with $q_0 = 1.1$.

In the case $Q = 1$, we did not find any initial condition such that the values of $\tau(t)$ are isolated from 0. Results obtained with $Q = 1$ and the same initial condition as previously, namely $(q, p, \xi_1, \xi_2) = (1.1, 0, 0, 0)$, are shown on Figure 7. We compare the theoretical distributions of the angular variable θ and of the amplitude variable $r = \sqrt{q^2 + p^2}$ (as given by the Gibbs measure (1.2)) with the empirical distributions obtained from the time trajectory. Since we work with $\beta = 1$, the theoretical distributions respectively read

$$f_{\text{theo}}^{\text{ang}}(\theta) = \frac{1}{2\pi} 1_{[0, 2\pi]} d\theta, \quad f_{\text{theo}}^{\text{amp}}(r) = r \exp\left(-\frac{r^2}{2}\right) 1_{[0, +\infty)} dr,$$

where $1_{[0, 2\pi]}$ is the characteristic function of $[0, 2\pi]$. The numerical distributions are denoted $f_{\text{num}}^{\text{ang}}(\theta)$ and $f_{\text{num}}^{\text{amp}}(r)$. They have been computed from a trajectory of length $T = 2.5 \cdot 10^6$, with a time step of $2.5 \cdot 10^{-3}$ (the trajectory is thus composed of 10^9 time steps), by partitioning the sampled interval into 100 bins (a cutoff of $r_c = 4$ has been used). Note that all distributions have been normalized so that their integrals are equal to 1.

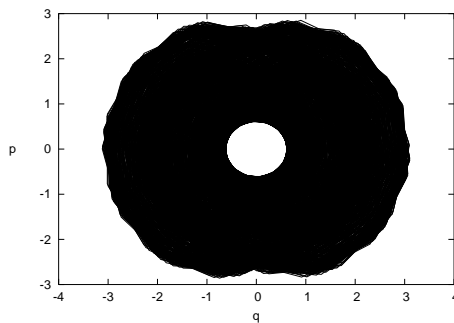


FIGURE 6. Projection on the (q, p) -plane of the trajectory of (4.5) with $\epsilon = 1/\sqrt{10}$, starting from the initial condition $(\theta, \tau, \alpha_1, \alpha_2) = (0, q_0^2/2, 0, 0)$ with $q_0 = 1.1$.

For the angular variable, we plot on Figure 7 both distributions $f_{\text{theo}}^{\text{ang}}(\theta)$ and $f_{\text{num}}^{\text{ang}}(\theta)$. We can see some small oscillations of the empirical distribution around the theoretical uniform distribution. Regarding the amplitude variable, it is more convenient to directly plot the difference $|f_{\text{theo}}^{\text{amp}}(r) - f_{\text{num}}^{\text{amp}}(r)|$. Again, we can see some oscillations, which are small (let us recall that the maximum value of $f_{\text{theo}}^{\text{amp}}(r)$ is $f_{\text{theo}}^{\text{amp}}(1) = 0.6$). We have checked that the error does not change when the time step is reduced, the total length T of the trajectory being kept fixed.

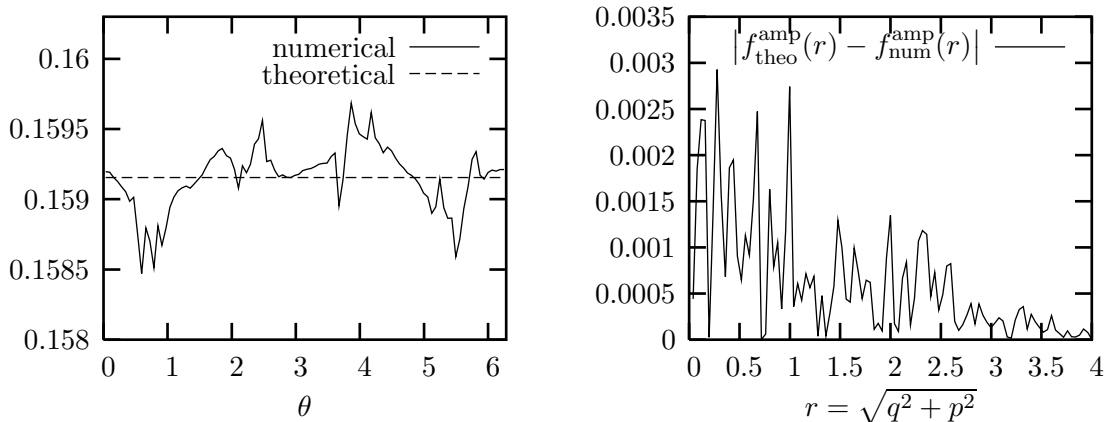


FIGURE 7. Left: Numerical and theoretical distributions of θ ; right: difference between the numerical and theoretical distributions of $r = \sqrt{q^2 + p^2}$. The numerical distribution is obtained from the simulation of (4.5) with $\epsilon = 1$, starting from the initial condition $(q, p, \xi_1, \xi_2) = (1.1, 0, 0, 0)$.

To study the evolution of the error with T (the time step being now kept fixed), the indicator we consider is the star discrepancy. Recall that the star discrepancy D_N of a sequence $x = \{x_n\}_{1 \leq n \leq N}$ with values in $[0, 1]^2$ is defined as [6]

$$D_N^*(x) = \sup_{y \in [0, 1]^2} \left| \frac{1}{N} \sum_{n=1}^N 1_{[0, y]}(x_n) - \text{Volume}([0, y]) \right|, \quad (4.7)$$

where, for 2-dimensional vectors y and z , we write $y \leq z$ when $y_i \leq z_i$ for all $1 \leq i \leq 2$, and note that $[0, y] = \{z \in [0, 1]^2, z \leq y\}$. The fact that $D_N^*(x) \rightarrow 0$ when $N \rightarrow \infty$ is equivalent [6, p.15] to the fact that, for any Riemann integrable function A defined on $[0, 1]^2$,

$$\lim_{N \rightarrow \infty} \frac{1}{N} \sum_{n=1}^N A(x_n) = \int_{[0, 1]^2} A(x) dx.$$

In addition, for functions A which have bounded variations $V_{\text{HK}}(A)$ in the sense of Hardy and Krause [11], the following error estimate holds true:

$$\left| \frac{1}{N} \sum_{n=1}^N A(x_n) - \int_{[0, 1]^2} A(x) dx \right| \leq V_{\text{HK}}(A) D_N^*(x). \quad (4.8)$$

If $A \in C^2([0, 1]^2)$, then its variation $V_{\text{HK}}(A)$ has a simple expression:

$$V_{\text{HK}}(A) = \int_{[0, 1]^2} \left| \frac{\partial^2 A}{\partial x_1 \partial x_2} \right| dx + \int_0^1 \left| \frac{\partial A}{\partial x_1}(x_1, 1) \right| dx_1 + \int_0^1 \left| \frac{\partial A}{\partial x_2}(1, x_2) \right| dx_2.$$

In view of (4.8), we can see that the convergence of $D_N^*(x)$ toward 0 implies the convergence of the empirical average of A towards its statistical average, and the rate of convergence of $D_N^*(x)$ gives information about the convergence rate of the observable average.

Here, we work with the discrepancy criterion

$$D_N^*({\theta}_n, r_n) = \sup_{(\theta, r) \in [0, 2\pi] \times [0, r_c]} \left| \frac{1}{N} \sum_{n=1}^N 1_{[0, \theta]}(\theta_n) 1_{[0, r]}(r_n) - \int_{\bar{\theta}=0}^{\theta} \int_{\bar{r}=0}^r \frac{\bar{r}}{2\pi} \exp\left(-\frac{\bar{r}^2}{2}\right) d\bar{\theta} d\bar{r} \right|, \quad (4.9)$$

where the sample (θ_n, r_n) is obtained by the numerical integration of the ODE with a time step of $\Delta t = 2.5 \cdot 10^{-3}$. We again set the cutoff amplitude at $r_c = 4$. Note that the integral that appears in (4.9) can be exactly computed. In practice, D_N^* is approximated by considering the supremum only over (θ, r) of the form (θ_k, r_l) with $\theta_k = 2k\pi/100$, $r_l = lr_c/100$, and $1 \leq k, l \leq 100$.

We have considered 8 different initial conditions, giving rise to 8 different samples (θ_n, r_n) , and for each of them, we have computed the star discrepancy D_N^* for several values of N . Results are shown on Figure 8, where we plot the mean of the computed discrepancies as a function of N . A least mean-square fit shows that the mean discrepancy decreases as $\frac{11.1}{N^{0.483}}$.

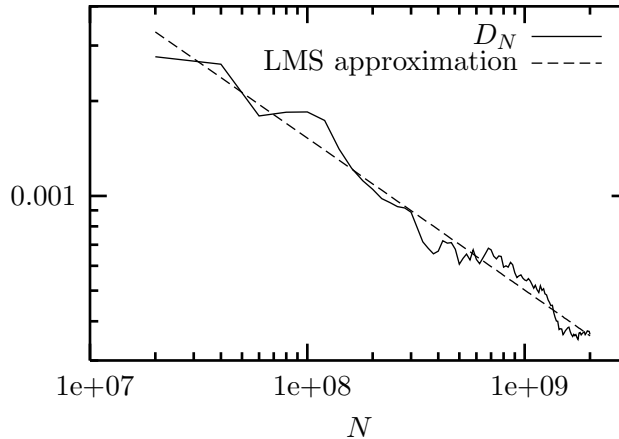


FIGURE 8. Star discrepancy (4.9) as a function of the sample size N , and comparison to the least mean-square fit $D_N^* \approx 11.1/N^{0.483}$.

We thus see from our numerical experiments with these thermostat masses and these initial conditions that the numerical distribution converges to the theoretical distribution, and the numerical results are thus consistent with ergodicity. However, more extensive numerical testing would be needed to assess whether this would be the case for any initial condition or any smaller thermostat masses.

5. ACKNOWLEDGMENTS

We thank Alain Chenciner and Jacques Fejoz for helpful suggestions on this research.

REFERENCES

- [1] S.D. Bond, B.J. Leimkuhler, and B.B. Laird. The Nosé-Poincaré method for constant temperature molecular dynamics. *J. Comput. Phys.*, 151:114–134, 1999.

- [2] C. Chicone. The monotonicity of the period function for planar Hamiltonian vector fields. *J. Differential Equations*, 69(3):310–321, 1987.
- [3] D. Frenkel and B. Smit. *Understanding Molecular Simulation, from algorithms to applications, 2nd ed.* Academic Press, 2002.
- [4] W.G. Hoover. Canonical dynamics: Equilibrium phase-space distributions. *Phys. Rev. A*, 31(3):1695–1697, 1985.
- [5] A.I. Khinchin. *Mathematical Foundations of Statistical Mechanics.* Dover, New York, 1949.
- [6] B. Lapeyre, E. Pardoux, and R. Sentis. *Méthodes de Monte Carlo pour les équations de transport et de diffusion.* Mathématiques et applications **29**. Springer, 1998.
- [7] B.J. Leimkuhler and C.R. Sweet. A Hamiltonian formulation for recursive multiple thermostats in a common timescale. *SIAM J. Applied Dynamical Systems*, 4(1):187–216, 2005.
- [8] G.J. Martyna, M.L. Klein, and M.E. Tuckerman. Nosé-Hoover chains: The canonical ensemble via continuous dynamics. *J. Chem. Phys.*, 97(4):2635–2643, 1992.
- [9] G.J. Martyna, M.E. Tuckerman, D.J. Tobias, and M.L. Klein. Explicit reversible integrators for extended systems dynamics. *Mol. Phys.*, 87:1117–1157, 1996.
- [10] D.A. McQuarrie. *Statistical Mechanics.* University Science Books, 2000.
- [11] N. Niederreiter. *Random Number Generation and Quasi Monte-Carlo Methods.* Society for Industrial and Applied Mathematics, 1992.
- [12] S. Nosé. A unified formulation of the constant temperature molecular dynamics method. *J. Chem. Phys.*, 81(1):511–519, 1985.
- [13] C.L. Siegel and J.K. Moser. *Lecture on Celestial Mechanics.* Springer, New York, 1971.
- [14] M.E. Tuckerman and G.J. Martyna. Understanding modern molecular dynamics: Techniques and applications. *J. Phys. Chem. B*, 104:159–178, 2000.

FREDÉRIC LEGOLL, INSTITUTE FOR MATHEMATICS AND ITS APPLICATIONS, UNIVERSITY OF MINNESOTA, 207 CHURCH STREET SE, MINNEAPOLIS, MN 55455, U.S.A. AND CERMICS AND LAMI, ENPC, 6 ET 8 AVENUE BLAISE PASCAL, 77455 MARNE LA VALLÉE, FRANCE
E-mail address: legoll@lami.enpc.fr

MITCHELL LUSKIN, SCHOOL OF MATHEMATICS, UNIVERSITY OF MINNESOTA, 206 CHURCH STREET SE, MINNEAPOLIS, MN 55455, U.S.A.
E-mail address: luskin@umn.edu

RICHARD MOECKEL, SCHOOL OF MATHEMATICS, UNIVERSITY OF MINNESOTA, 206 CHURCH STREET SE, MINNEAPOLIS, MN 55455, U.S.A.
E-mail address: rick@math.umn.edu